Vol. 45, No. 4 (2023) 650-663, DOI: 10.24874/ti.1497.06.23.09

Tribology in Industry

www.tribology.rs

RESEARCH

Parametric Design Optimization of Convergent Textured Thrust Bearing in THD Behaviour

Mertad Omar[a,b,*], Youcefi Abdelkader[a], Maamar Fatouma[b], Mostefa Kouider[c]

[a]*Faculté de Génie Mécanique, Université des Sciences et de la Technologie d'Oran Mohamed Boudiaf, USTO-MB, BP 1505 El M'naouer, 31000 Oran, Algeria,*
[b]*Satellite Development Center (CDS), Space Mechanical Research Department, BP 4065 Ibn Rochd USTO, Oran 31001, Algeria,*
[c]*Laboratory of Mechanical Engineering, Materials and Structures, Tissemsilt University, Benhamouda BP 182, Tissemsilt 38010, Algeria.*

Keywords:

Converging textured thrust bearing
Optimization
Load capacity
Maximum temperature
Friction torque

* Corresponding author:

Omar Mertad
E-mail: omar.mertad@univ-usto.dz

Received: 15 june 2023
Revised: 26 July 2023
Accepted: 22 August 2023

A B S T R A C T

Textured thrust bearing is a technological means capable of providing higher performance compared to untextured bearing. This paper presents a parametric design optimization with thermohydrodynamic (THD) behaviour of textured thrust bearing in a range of convergence ratios. The bearing consists of eight pads (stator), film fluid and a collar (rotor). The main objective of this optimization is to provide higher load capacity, to relatively minimize the maximum temperature of the pad and the friction torque. To this aim, we perform a 3D computational fluid dynamics model for convergent thrust bearing with individual angular sector shaped texturing with a flat bottom profile pad, by using ANSYS. CFX, and considered a thermal effect.

1. INTRODUCTION

Energy efficiency is always a big issue for engineering applications, such as thermal and mechanical losses. Friction is considered today as a topical loss for industrialists and engineers.

In order to reduce friction torque, an effective way for controlling friction at the oil-lubricated interface has been shown to be surface texturing. These surface texturing are commonly deployed in bearings and seals. In addition, the fluid film can provide additional forces with these textured surfaces and improve the hydrodynamic behaviour of the system.

Advanced based-treatment surface technics allow the implementation of textures with dimensions of a few microns or even less [1]. For more than 50 years numerous researches based on numerical modeling using Reynolds equations have been developed for the use of textures. The main performance in these researches is the load carrying capacity and the friction torque. Marian. V. G, Gabriel [2] demonstrate theoretically and experimentally the potential of texture performance. Dobrica. M. B, and Fillon. M [3] investigate the validity of Reynolds equation and inertia effects in textured sliders of infinite width. They show the effect of Reynolds number and texture characteristics in the accuracy of the results. At present, to obtain the best bearing performance, researchers are mostly focused on the optimization of the texture patterns on the stator surface combining the Reynolds equation with optimization tools. Papadopoulos. C. I [4][5] present an optimization of trapezoidal and rectangular dimples on a micro-thrust bearing, the comparison between these results and the results of pocket bearing and tapered land in the work of Fouflias. D. G [6] shows that the textured thrust bearing gives a better friction characteristic. The work of Papadopoulos et al [7] allows to show that the load capacity increases with the texture circumferential and radial extent up to an optimum value, when the dimple depth should be close to the film thickness. The approach of Dadouche. A, Fillon [8][9] analyse the thermal effect and the influence of temperature increase on the local viscosity of the thrust bearing. The work of Gropper.D, Harvey. J and Wang. L, [10] [11] present a Numerical analysis and optimization of surface textures for a tilting pad thrust bearing. The obtained results show that a set of parameters depends on the operating conditions and texture density. However, this set is independent of the optimization goal. Also, the optimum texture extent in the circumferential direction is largely independent of rotational speed and texture density but does depend on the specific bearing load and the optimization objective.

In this paper, we aim at maximizing the load-carrying capacity, minimizing the maximum pad temperature, and minimizing the friction torque. To do this, we introduce an approach based on set of geometric parameters that are optimized according to ANSYS software.

The rest of this paper is organized as follows: In Section 2, the problem definition and computational approach are first defined. In Section 3, design and parameterization are then presented. In section 4, obtained results and discussion are described. Conclusion are given in Section 5.

2. PROBLEM DEFINITION AND COMPUTATIONAL APPROACH

In this section, we present the problem definition and our validation model for the Non-dimensional load carrying capacity, maximum pad temperature and friction torque.

2.1 Converging thrust bearing geometry

Figure 1 illustrates the geometry of converging thrust bearing with individual angular sector shaped texturing with a flat bottom profile pad. The moving wall generates shear forces, exerting motion on the fluid, which flows from the bearing inlet to the outlet.

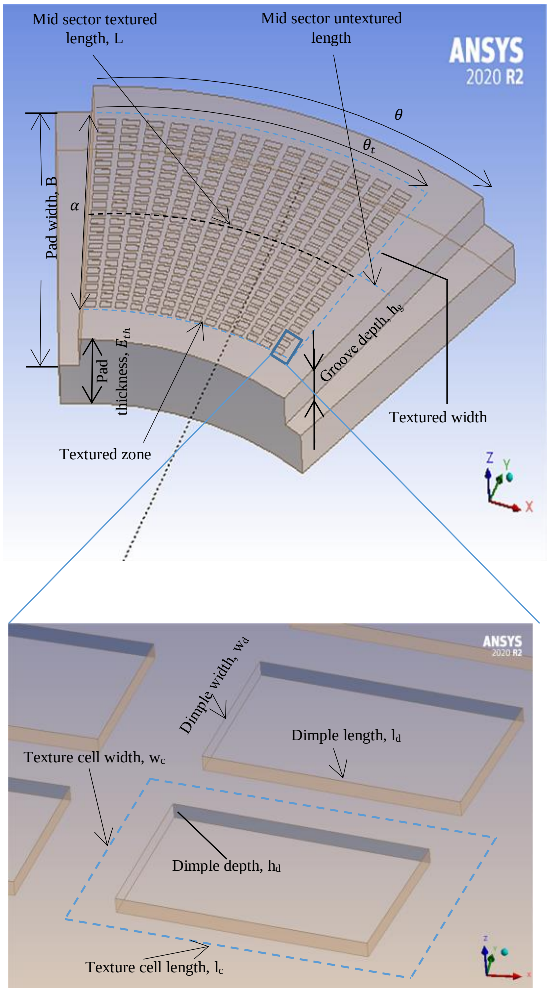

Fig. 1. The geometry of the thrust bearing with individual angular sector-shaped texturing cells.

The cumulative pressure due to the convergent geometry and the presence of dimples exerts equilibrium forces on the fluid-wall interfaces of the bearing (pad, rotor). The inner radius of slider bearing R_i is 51,55mm, its outer radius is R_{out} is

97,55mm and a thickness of 10mm. The groove of the oil supply channel has an angular sector of 7^0 and 4,1mm of depth. This convergent thrust bearing consists of eight pads; each bearing lies between two grooves. The pad length at the mid-sector of the bearing is 49.44mm. We consider in this paper, the textured extent in circumferential and radial directions are variables from 0 to 1 (one of the objectives of this optimization study). The film thickness changes from the inlet height h_1 to its value h_0 at the outlet; their value is controlled by the convergence ratio $k=(h_1-h_0)/h_0$. The minimum film thickness h_{min} is constant in all cases, equal to 30μm. The dimple number is 14 in the circumferential direction and 23 in the radial direction. Each textured cell is defined by the cell width, (wc), the cell length (lc), the dimple width (w_d), the dimple length (l_d), and the dimple depth (h_d). These dimensional geometric parameters are controlled by the texture density in the circumferential direction $\rho_{cir,}$ the texture density in the radial direction ρ_{rad}, and the dimple depth, h_d. Table 1 lists the complete data set regarding the basic bearing geometry. The thrust collar surface is assumed planar and smooth.

Table 1. Thrust bearing geometry characteristics.

Item	Symbol	Value
The inner radius of the pad	R_i	51,55 mm
The outer radius of the pad	R_{out}	97,55 mm
The mean radius of the pad	R_m	74,55 mm
Pad width	B	46 mm
Groove angle/depth	G_{ang}/ h_g	7^0/4,1 mm
Pad length at mid sector	L	49,44 mm
Pad thickness	E_{th}	10 mm
Specific heat capacity of the pad	$C_{p(pad)}$	380 J/kg. K
Thermal conductivity of pad	λ_{pad}	65 w/m. K
Collar thickness	C_{th}	15 mm
Specific heat capacity of the pad	$C_{p(collar)}$	490 J/kg. K
Thermal conductivity of pad	λ_{collar}	50 w/m. K

2.2 Governing equations and CFD analysis

In this study, we deploy the laminar flow with THD behaviour. Cavitation does not usually occur in textured inclined pad thrust bearings as the overall convergence builds up enough pressure to prevent pressures from falling below the cavitation pressure. The conservation equations for steady incompressible and non-isothermal flow, with zero gravitational and other external body forces, are as the following:

Mass conservation equation

$$\nabla V = 0 \tag{1}$$

Momentum equations

$$\rho V.\nabla = -\nabla P + \nabla.(\mu \nabla V) \tag{2}$$

Energy equation, fluid domain

$$\rho C_p \, V.\nabla T = \nabla.\lambda f \nabla T - \tau \tag{3}$$

Energy equation, solid domain

$$\nabla.(\lambda_s \nabla T) = 0 \tag{4}$$

Where P is a reference pressure flow, V is the velocity vector, T is the temperature, ρ is the fluid density, μ is the dynamic viscosity, C_p is the specific heat capacity, λ_f and λ_s are respectively the thermal conductivity of fluid and solid, and τ is the viscous stress tensor. Equations (1)-(4) are solved with the CFD code ANSYS CFX 20. Table 2 gives the following lubricant properties. The oil used in this model is ISO VG 32, the temperature-dependent oil viscosity is considered in this simulation. The viscosity temperature correlations are the Groof relation:

$$\mu(T) = \mu_0 . e^{-\beta(T-T_0)} \tag{5}$$

Table 2. Lubricant properties.

Item	Symbol	Value
Density	ρ	870 Kg/m³
Dynamic viscosity at 40^0C	μ_{40}	0,0285 Pa. s
Specific heat capacity	$C_{p(oil)}$	1960 J/kg. K
Thermal conductivity	λ_{oil}	0,13 w/m. K

Where μ_0 is the dynamic viscosity at a given temperature, T is the absolute temperature, β specific to each lubricant, called the thermo-viscosity coefficient, and can be determined from the known viscosity at two different temperatures.

2.3 Discretization and Boundary Conditions

Figure 2 summarizes the generated mixed mesh model, with hexahedral elements for the fluid domain and tetrahedral elements for the pad (solid domain). The typical 3D mesh generated consists of approximately 12×10^6 total finite elements and 7×10^6 nodes between fluid and solid domains. The minimum film thickness has a minimum of 12 cell layers in the untextured region and also 12 cell layers throughout the dimple depth. The grid is denser in the near-wall region. In order to minimize the convergence criteria, we perform an efficiency model that considers the pressure and load capacity parameters. In addition, we analyze the evolution of the two last parameters by increasing the nodes number of mesh up to meet the optimum value for each parameter. Figure 3 shows the results of the calculations.

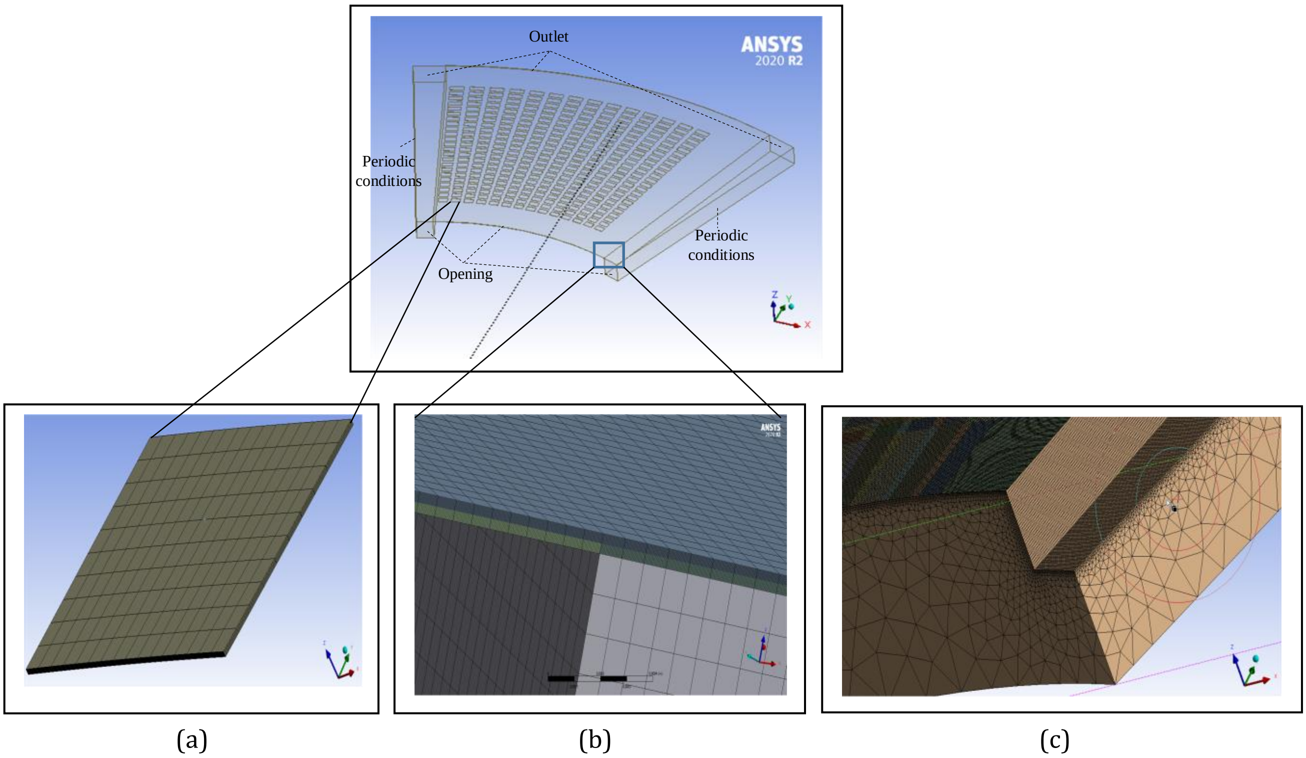

Fig. 2. (a) Dimple discretization, (b) Film discretization, (c) Pad discretization.

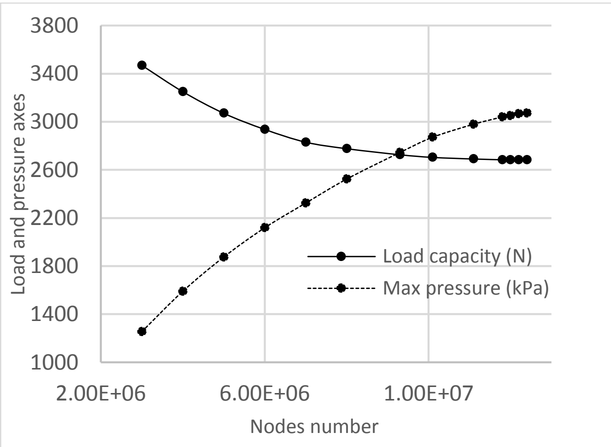

Fig. 3. Evolution of max pressure and max load according to the nodes' number of the mesh.

The textured wall region is stationary and the upper wall (rotor interface) is moving at a constant angular velocity, with no-slip conditions at both wall surfaces. Table 3 presents the operating parameters used in this simulation.

Rotational periodicity is implemented for corresponding points of the inflow and outflow areas of the fluid domain.

Table 3. Operating parameters.

Item	Symbol	Value
Rotational speed	N	5000 rpm
Minimum film thickness	h_{min}	30 µm
Feeding oil temperature	T_{in} *(opening)*	40 ^{0}C
Feeding pressure	P_{fe} *(opening)*	10^5 Pa
Ambient pressure	P_{amb} *(outlet)*	0 Pa

At the fluid–pad interface and fluid-collar interface, continuity of temperature and heat flux is considered. In Table 4 and Table 5 the thermal boundary conditions of pad and collar surfaces are summarized respectively.

Table 4. Pad thermal boundary conditions.

Surfaces	Boundary conditions
Bottom surface	Heat transfer coefficient:200 w/m^2. K, T=40 ^{0}C
Inner surface	Heat transfer coefficient:200 w/m^2. K, T=40 ^{0}C
Outer surface	Heat transfer coefficient:25 w/m^2. K, T=40 ^{0}C
Sides	Rotational Periodicity

Table 5. Collar thermal boundary conditions.

Surfaces	Boundary conditions
Top surface	Heat transfer coefficient:100 w/m². K, T=40 ⁰C
Inner surface	Heat transfer coefficient:100 w/m². K, T=40 ⁰C
Outer surface	Heat transfer coefficient:100 w/m². K, T=40 ⁰C
Sides	Rotational Periodicity

The friction torque and the load-carrying capacity supported by the bearing exerted on the rotor are calculated by integrating the shear stress, τ, and field of the pressure, p, respectively, over the rotor surface.

$$F = N_p \int p.ds \tag{6}$$

$$St = \int \tau.r.ds \tag{7}$$

2.4 THD modelling validation

In order to validate the CFD model, we need to compare the computational results of load-carrying capacity, temperature and friction torque as shown in Figures (4.a, 4.b and 4.c).

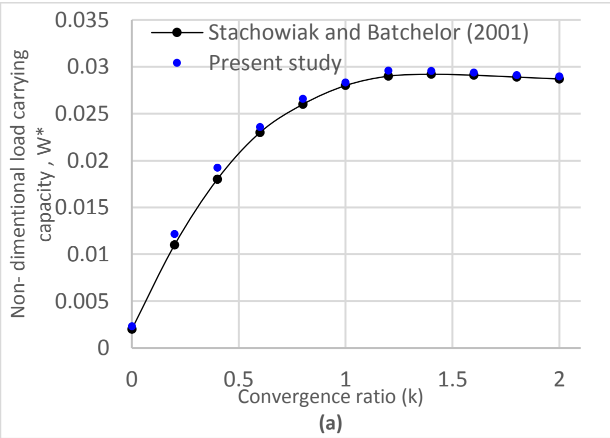

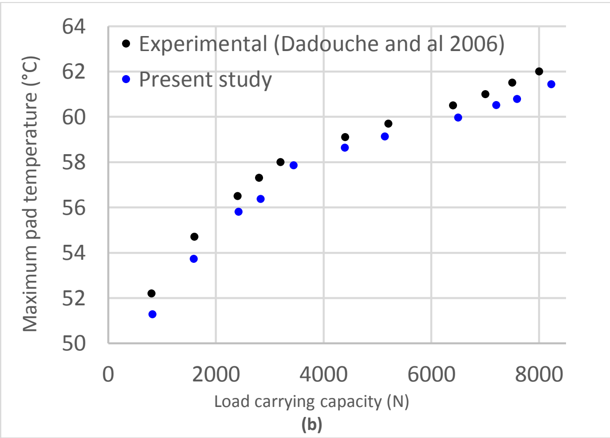

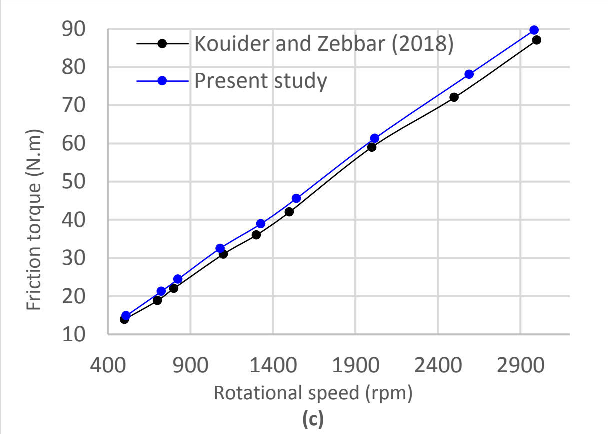

Fig. 4. Validation of present CFD results against literature: (a) Computed non-dimensional load carrying capacity versus convergence ratio of the smooth slider: (b) maximum temperature versus bearing load (2600 RPM): (c) Friction torque versus rotational speed (RPM) for a dimple bearing.

In the first step, calculations are performed for 3-D smooth converging sliders of B/L=1, the convergence ratio values and for the processed of the load-carrying capacity. The obtained results are compared to the published data of Stachowiak and Batchelor [12]. In the second step, the obtained results related to the temperature parameter are also compared to the experimental results of the work of Dadouche et al [13] of tapered-land bearing geometry. The third step, the comparison between our obtained results related to the friction torque and the results of Kouider and Zebbar [14] is achieved.

2.5 Untextured thrust-bearing performances

Figures 5 (a), (b), and (c) show respectively the evaluation of thrust bearing load capacity, the maximum pad temperature, and the friction torque as a function of convergence ratio (k) for a smooth thrust bearing (without texture) for a minimum film thickness h_{min} of 30µm. Figure 5(a) allows to deduce that the generated load increases with the convergence ratio k_{opt} up to an optimal value of k_{opt}=1,246. Thus, it decreases after this k_{opt}=1,246. In Figure 5 (c), the same trend is observed for the friction torque. On the other hand, the maximum temperature at the pad film interface is inversely proportional with the increase of the convergence ratio (k) which is appropriate as a performance for the system. However, the convergence ratio k is not taken into consideration after the optimum value of k_{opt} =1,246 because of the load capacity decrease.

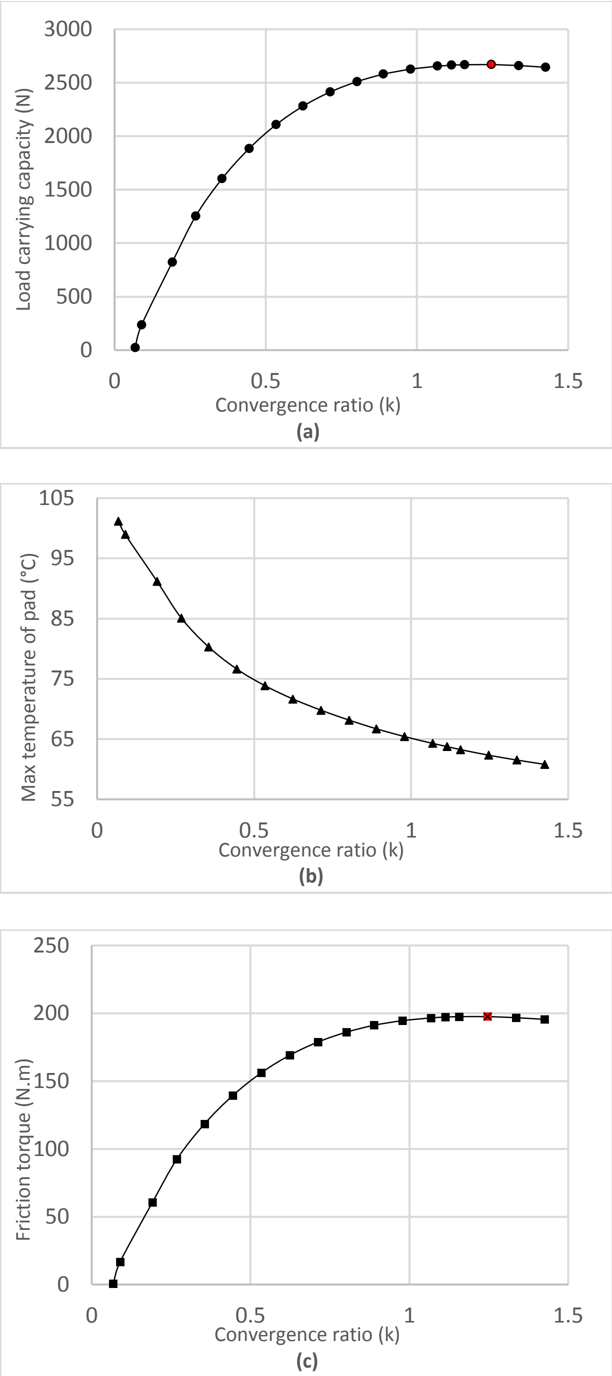

Fig. 5. Computed values of: (a) load capacity, (b) maximum temperature of the pad and (c) friction torque versus convergence ratio (k) for untextured bearing.

3. DESIGN AND PARAMETERIZATION

In this section, we present our technic to design and to configure the convergence thrust bearing in THD behaviour. The geometry of the thrust bearing with individual angular sector shaped texturing with a flat bottom is parameterized to lead to a sensitivity analysis. To do this, we define a set of variable parameters of the geometry as follows:

- the angular span of the textured zone θ_t(°) (textured extent in the circumferential direction).
- the textured extent in the radial direction (α).
- the dimple depth (h_d).
- the dimple density in the circumferential direction (ρ_{cir}).
- the dimple density in the radial direction (ρ_{rad}).
- the convergence ratio (k).

As explained above, our main idea is guided by the optimization of textured geometry for the maximum load capacity, that we called (F). Thus, it is considered as an increasing function of the convergence ratio (k) up to an optimal value, minimizing the maximum temperature of the pad and minimizing the friction torque. In order to achieve this, we propose a multi-objective optimization based on a set of the following guidelines steps:

Step 1: Calculate the performances of the untextured thrust bearing with the fixed conditions of operation (h_{min}, rotational speed)

Step 2: To reduce the number of combinations between the design variable parameters in the first step of the optimization process, three parameters it should be fixed with any value chosen randomly e.g.: textured extent in the radial direction α = 0,75; dimple density in the circumferential direction ρ_{cir}=0,714, the dimple density in the radial direction (ρ_{rad} =0,666); and a combination between three other geometrical variables (θ_t), (h_d), and (k) is performed.

Step 3: If the three parameters (load, temperature, friction torque) are optimized, the optimization will get its objective.

Step 4: If the three parameters are not optimized, the dimple density should be increased in the circumferential density until the first objective (load carrying capacity) is optimized and verify the two other parameters (temperature and friction torque) with the untextured bearing parameters.

(a) If the two parameters are optimized, the optimization is finished.

(b) If not, the dimple density in the radial density should be increased with different values until the temperature and the torque are optimized by selecting the first value which optimizes the two parameters (see Figure. 12.c below).

Step 5: The effect of the radial extent should be verified with these dimple densities to see if the three parameters can be optimized furthermore by verifying these results with the last obtained results.

In this paper, we consider the convergence ratio (k), as an independent variable as well as an objective function of the problem.

4. OPTIMIZATION RESULTS

In this section, we present the obtained results of the parametric optimization.

4.1 Optimum load-carrying capacity

Figure 6 presents the obtained optimal load-carrying capacity of textured and untextured bearing for radial extent α 0,75; circumferential density ρ_{cir}=0,714 and radial density ρ_{rad} =0,666 versus convergence ratio k for the same operation conditions and the same minimum film thickness of 30μm. The dashed and solid lines correspond respectively to optimized textured and untextured bearings as a function of convergence ratio. Based on Figure 6, some observations can be drawn:

- For both bearings textured and untextured patterns, the load capacity increases with the increase of convergence ratio up to an optimal value, k_{opt}=1,131 for textured bearing and k_{opt}=1,246 for untextured bearing.
- The improvement in load capacity between textured and untextured bearings is drastic for a small value of convergence ratio. This improvement decreases with the increase of convergence ratio (k).
- At the optimum convergence ratio, the improvement of load carrying capacity reaches 2,97% and 3,2% for the same convergence ratio of k=1,131 between textured and untextured bearings.
- The textured patterns always decrease the optimum convergence ratio, which is explained by the circulation of the fluid on the texture pockets, which favors the increase of the local pressure and leads to a reduced convergence ratio compared to that of the untextured bearings.

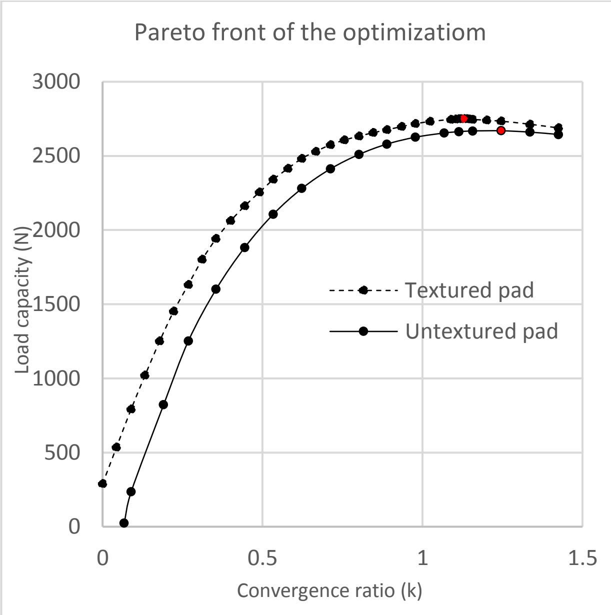

Fig. 6. Optimal load carrying capacity of textured and untextured bearing for (α = 0,75; ρ_{cir}=0,714 and ρ_{rad} =0,666) versus convergence ratio (k).

Figure 7 (a) shows the computed values of optimal friction torque versus the load capacity, using the Pareto front of optimization. As an optimization objective, the load carrying and friction torque are selected to obtain a design providing a maximum load and minimum friction torque. The red point shown on the low right boundary presents the best set of samples keeping the maximum load-carrying capacity with the value of 2748,78 N as a result of this CFD simulation. Figure 7 (b) and Figure 7 (c) illustrate respectively the optimal dimple depth and the optimal angular span texture versus convergence ratio. We can deduce that the optimal dimple depth and optimal angular span are practically dependent on the convergence ratio (k). Furthermore, we consider from below that a smaller dimple depth is favoured at an increasing value of k (see Figure 7(b)) unlike for optimal angular span. The optimal dimple depth value in this study is 18,67μm and the optimal angular span is 32,48° corresponding to 85,47% as textured extent in a circumferential direction.

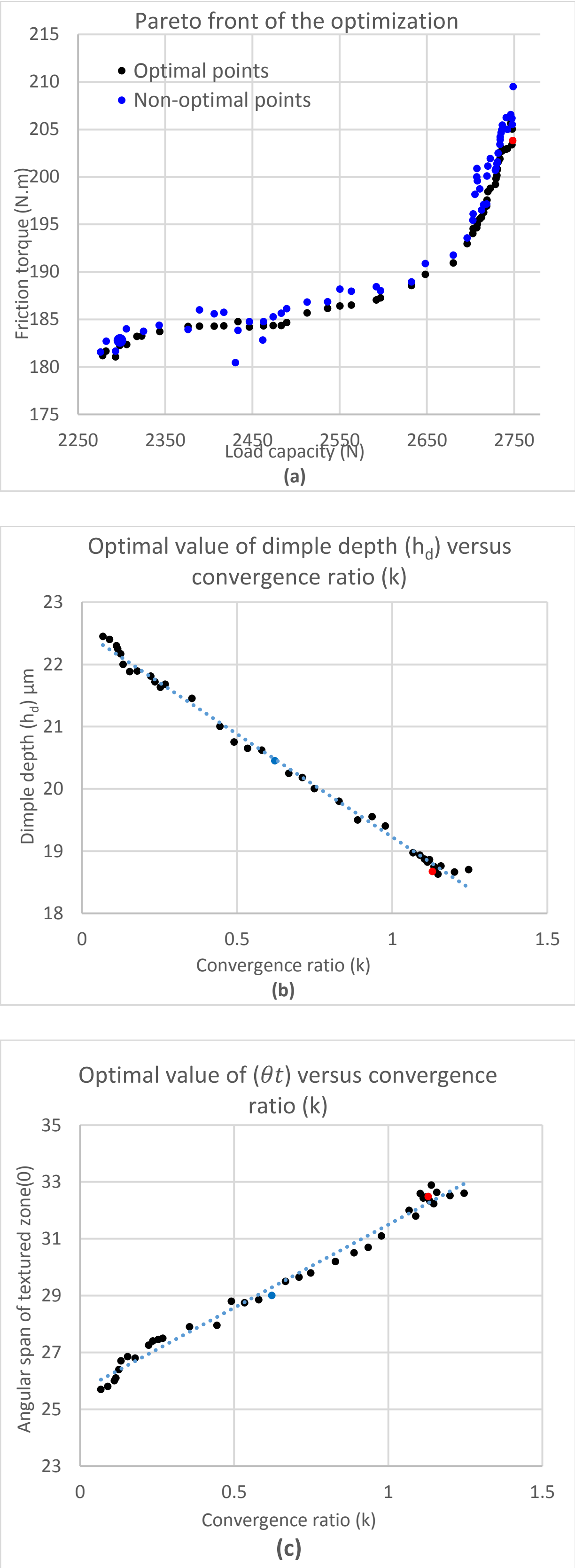

Fig. 7. Computed values of: (a) optimal friction torque (St) versus load capacity, (b) (c) optimal values of dimple depth (h_d), and angular span of the textured zone θ_t(°) (textured extent in a circumferential direction), versus convergence ratio (k).

4.2 Optimum circumferential texture extent and dimple depth

Figure 8 and Figure 9 allow to describe the details of the obtained results related to the optimization experimentation in terms of textured extent in circumferential direction and pressure build-up.

Thus, we give an example of two different convergence ratios to find the optimal extent in the circumferential direction. Then, we provide the corresponding pressure contours that show the combinations between geometrical parameters. Each plot point in Figure 6 for textured bearing is computed by set of combinations between geometrical parameters.

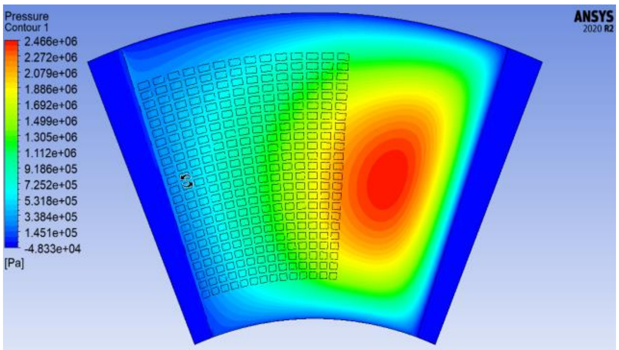

(a) θ_t=22,5° ; F=2430,6 N ; T=72,75°c ; St=180,42 N.m

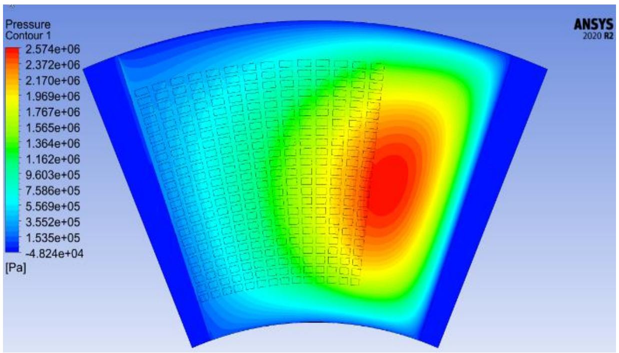

(b) θ_t=26° ; F=2462,3 N ; T=72,47°c ; St=182,79 N.m

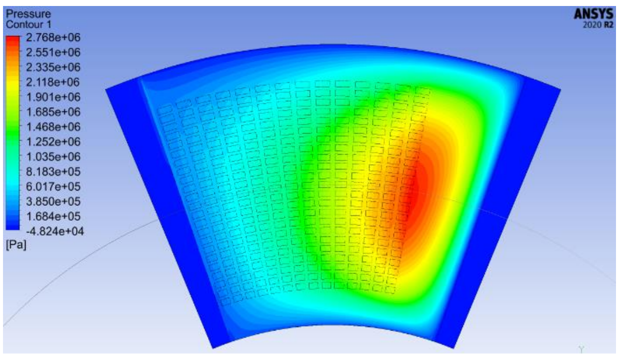

(c) θ_t=29° ; F=2483,1 N ; T=72,19°c ; St=184,34 N.m

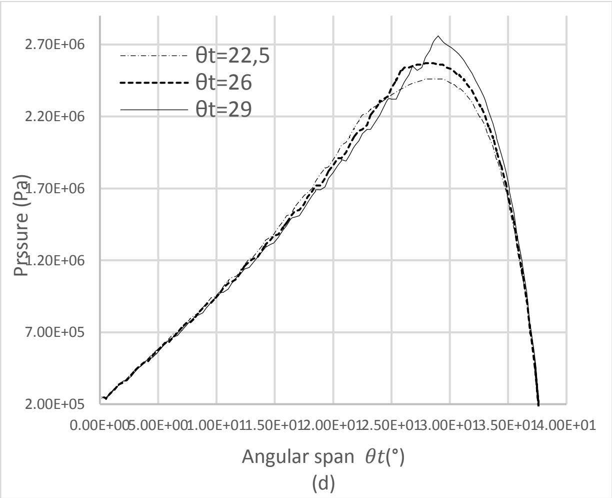

Fig. 8. (a)-(b) and (c) Corresponding pressure contours of respectively: θ_t=22,5°; θ_t=26° and θ_t=29°, (d)Pressure distribution of three different angular spans of the textured zone for convergence ratio k=0,623.

Figure 8, Figure 9, Figure 10 and Figure 11 allow some remarks:

- We can observe, on the one hand, that for the same convergence ratio k, the maximum temperature decreases with the increase of the circumferential extent even if θ_t exceeds θ_{opt}. Then, on the other hand, the friction torque increases with the increase of the circumferential extent until the optimal value and will decrease after this value (same trend as the load).
- We deduce that around ½ of the pad should be textured to minimize the friction torque for a small convergence ratio.
- We recommend that in order to minimize the maximum temperature, a high lubricant supply is needed. We can obtain a such lubricant supply by increasing the convergence ratio. At this moment, the pressure and maximum temperature points are closer, which is also explained by the great influence of the circumferential extent. (see Figure.10.)

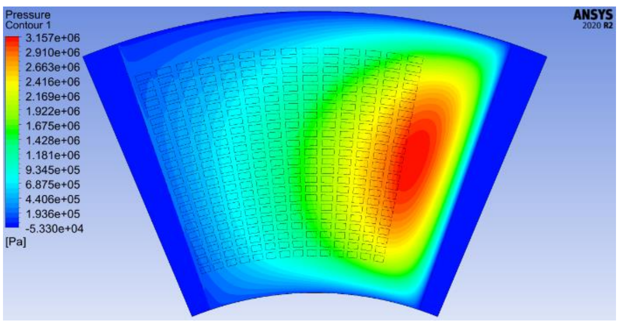

(a) θ_t=29,96° ; F=2736,8 N ; T=64,78°c ; St=202,92 N.m

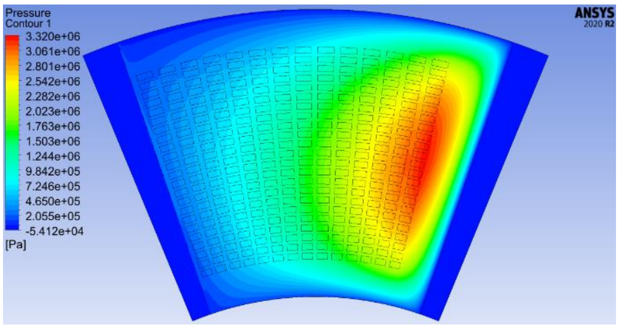

(b) θ_t=32,48° ; F=2748,78 N ; T=64,52°c ; St=203,81 N.m

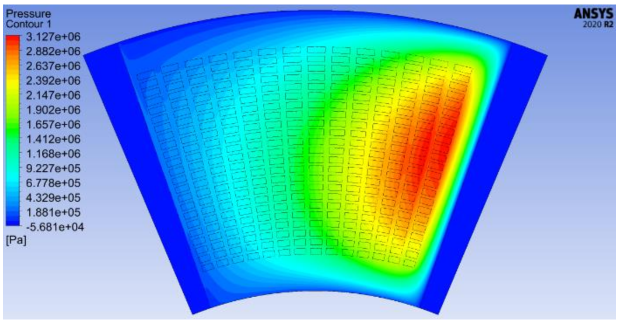

(c) θ_t=35° ; F=2707,6 N ; T=63,9°c ; St=200,85 N.m

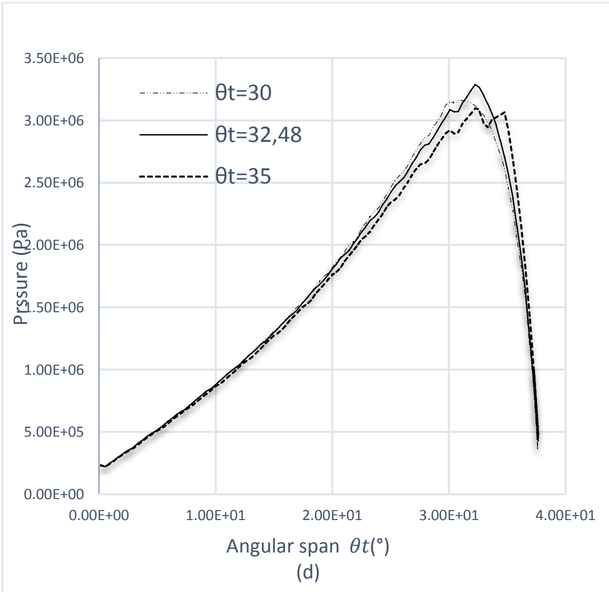

Fig. 9. (a)-(b) and (c) corresponding pressure contours of respectively: θ_t=29,96°;θ_t=32,48° and θ_t=35°, (d)Pressure distribution of three different angular spans of the textured zone for convergence ratio k=1,131.

- For the optimal case of k=1,131, the optimal dimple depth is h_d=18,67µm as shown in Figure.11.
- From above, we can consider that the optimum texture depth decreases with an increase in load, and only varies slightly with a change in applied specific load.

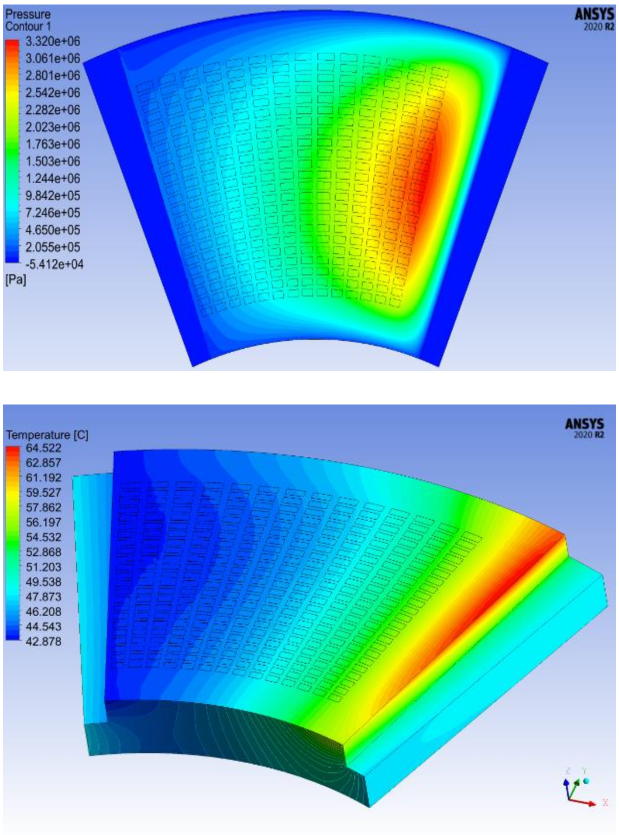

Fig. 10. Corresponding pressure and temperature distribution of the optimal case for θ_t=32,48°and convergence ratio k=1,131

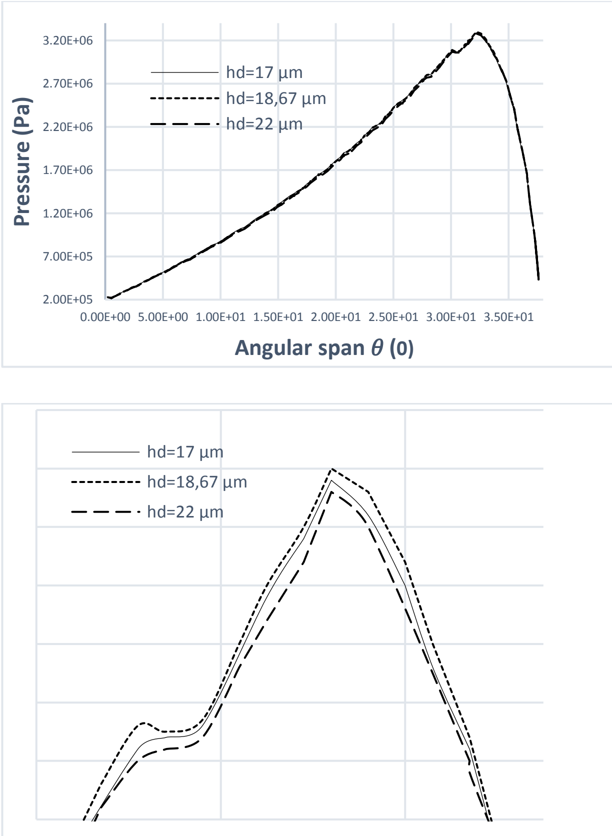

Fig. 11. Corresponding pressure contours for several dimple depth of the optimal case for θ_t=32,48°and convergence ratio k=1,131

Table 6. Relative change in parameters due to the texturing surface.

	h_{untex} (µm)	h_{tex} (µm)	F (N)	T_{Untex} (^{0}C)	T_{Tex} (^{0}C)	St_{Untex} (N.m)	St_{Tex} (N.m)	ΔT (%)	ΔSt (%)
K=0,623	28,74	30	2430,6	72,547	72,75	181,514	180,42	0,2798	-0,603
	28,487	30	2462,3	72,73	72,47	184,024	182,79	-0,357	-0,670
	28,324	**30**	**2483,1**	**72,849**	**72,19**	**185,671**	**184,34**	**-0,904**	**-0,716**
K=1,131	29,279	30	2736,8	64,19	64,78	206,47	202,92	0,919	-1,719
	29,167	**30**	**2748,78**	**64,25**	**64,52**	**207,55**	**203,81**	**0,42**	**-1,802**
	29,55	30	2707,6	64,03	63,9	203,84	200,85	-0,203	-1,466

Table 6 shows the relative change in parameters due to texturing, allowing an overall assessment of the texture design. We can see that for the convergence ratio k=0,623, the parameters: maximum temperature and friction torque are optimized, but for the optimal case with convergence ratio k_{opt}=1,131 only the friction torque is optimized. These optimization values are insufficient in terms of percentage. Therefore, in the following sub-sections, we need to vary other parameters.

4.3 Effect of radial density

We consider the radial density as a new parameter of our optimization function (defined based on the load capacity, the friction torque, and the maximum temperature). The obtained results related in terms of radial density are presented in Figure 12 (a, b, and c). We observe that the load-carrying capacity is a continuously increasing function of texture density (Similarly to the results of reported in Dobrica. M. B, and Fillon. M [3]). The same trend is observed for the friction torque and even the relative improvement with the increasing of the radial density as shown in table 7.

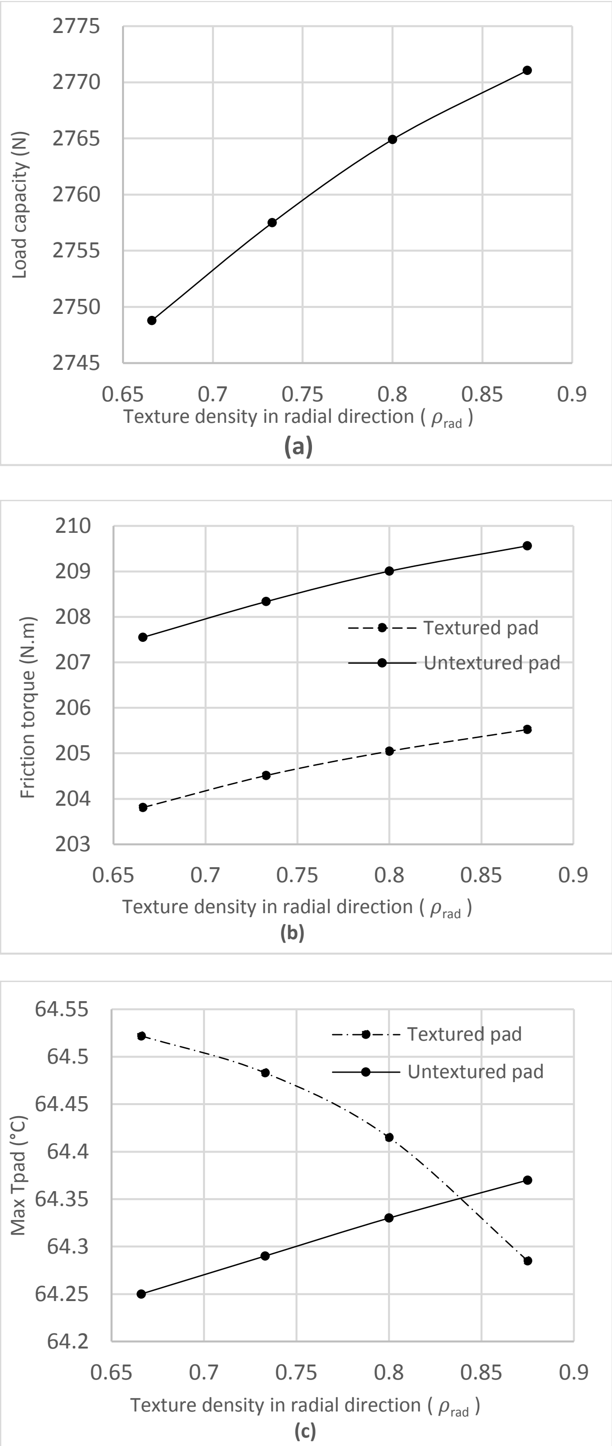

Fig. 12. (a)-(b) and (c) Corresponding plots contours of respective load, friction torque, and maximum temperature versus function of radial density.

Table 7. Relative change in parameters due to the radial density variation.

	ρ_{rad} (%)	F (N)	ΔT (%)	ΔSt (%)
K=1,131	66,66	2748.78	0,42	-1,802
	73,3	2757.48	0,279	-1,835
	80	2764,9	0,139	-1,893
	87,5	**2771,05**	**-0,139**	**-1,927**

Contrary to the load and the frictional torque, we can see that the maximum temperature decreases with the increase of the radial density (see Figure 12.c). However, the relative improvement still not reached when the radial density is lower than 84%. Beyond this value the improvement can be reached (see Figure12.c and Table 7). In this optimization study, we chose a new value of the radial density ρ_{rad} = 87,5%. The convergence ratio is slightly decreased by approximately 3,18% (k_{opt} = 1,095). In addition, the circumferential extent (θ) is almost independent of texture density and the optimum texture depth depends on the texture density, where a higher density entails deeper textures (h_{dopt} = 19,25μm).

4.4 Effects of circumferential density and radial texture extent

Figures.13. (a)-(b) and (c) describe the effect of radial texture extent and circumferential density on load capacity, relative friction torque, and relative maximum temperature respectively. Figure. 13.a shows that the load increases with increasing circumferential density and with radial extent up to an optimum value in this case α_{opt}=0,75 (75%) and it begins to decrease after this value similarly to the optimum extent in the circumferential direction. For our case study (0,714 as circumferential density: see the black curve) the improvement of the load reaches 4,04% and 6,1% for the circumferential density of 0,9. The same trend for the friction torque as for the load capacity (see Figure.13. b).

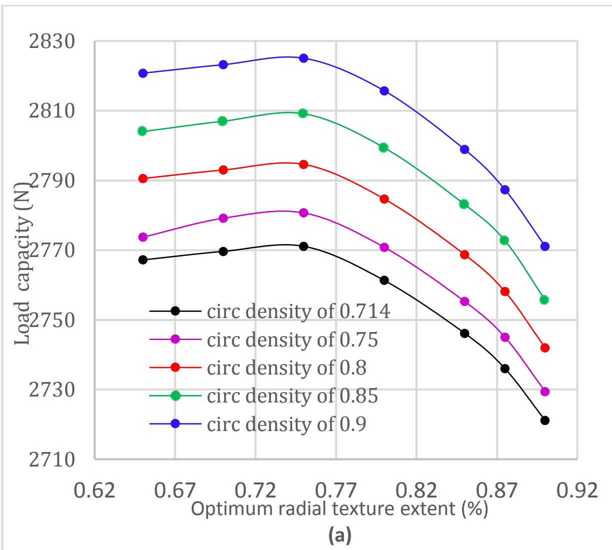

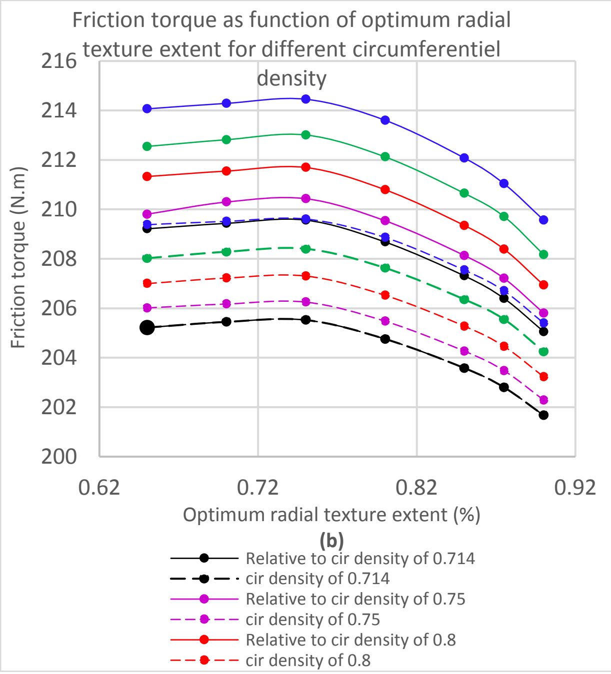

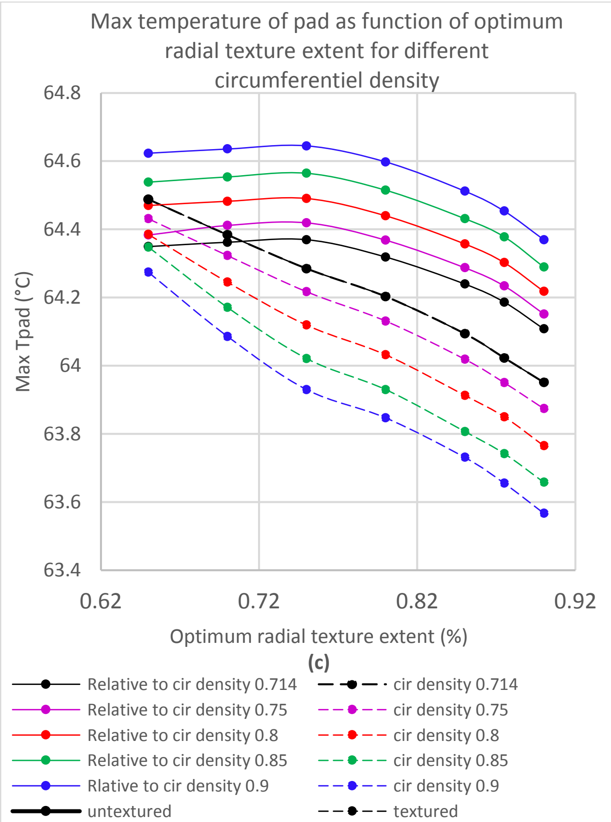

Fig. 13. (a)-(b) and (c) Corresponding plots contours of respective load, friction torque, and maximum temperature versus function of circumferential density and radial texture extent.

We have to mention that the relative maximum temperature decreases simultaneously with the increase of the circumferential density and with the increase of the radial extent for the same radial density.

The improvement is well observed each time the circumferential density increase (see Figure.13.c). One of the main reasons of the obtained improvement is physically related to a high inflow lubricant supply.

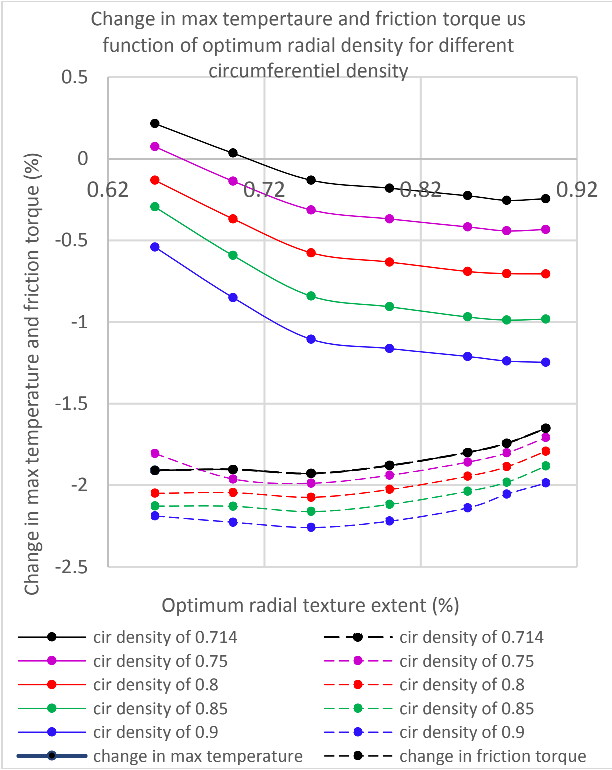

Fig. 14. Change in max temperature and friction torque versus function of circumferential density and radial texture extent.

Figure 14 illustrates two types of change according to the optimum radial texture extent. Thus, the continuous lines depict the maximum temperature change that impacts the pad, while the dashed lines depict the friction torque change. We recall our objective is to find the set of higher values which is related to the optimum radial texture extent. Following that, any temperature decrease becomes impossible when the optimum radial texture extent value is less than 70% for circumferential density value of 0,714 (black continuous line in Figure 14), and optimum radial texture extent value is less than 66,5% for circumferential density value of 0,75 (pink dash line). Moreover, Figure 14 allows us to agree that a relatively high texture extent value in a radial direction is approximately 87,5%. In fact, the reason behind this agreement is more the extent in the radial direction increases, the higher lubricant inflow, which allows to favor the cooling and to reduce the maximum temperature. 75% when the objective is a minimization of the friction torque and maximization of the load capacity.

5. CONCLUSION

This paper deals with the issues of the temperature minimization, the load carrying capacity increase, and friction torque minimization. To this aim, we have introduced a parametric design optimization on thermo-hydrodynamic behaviour of textured thrust bearing in the range of convergence ratios. Several combinations of geometric parameters of textures are experimented by the use of a CFX code. The obtained results allow us to provide the following conclusions:

- The improvement in load capacity between textured and untextured bearings is better for a small value of convergence ratio. This improvement decreases with the increase of the convergence ratio.
- Interestingly, the studied texture patterns always decrease the optimum convergence ratio.
- The improvement in load capacity also depends on the value (L/B) [5], in our case this ratio is close to 1, and this is why the improvement is around 4%.
- The optimum texture depth depends on the applied load.
- It is notable that the optimum circumferential texture extent θ_{opt} is almost independent of the texture density
- The increase in density minimizes the maximum temperature and also the increase in extent in both circumferential and radial directions.
- To optimize the maximum temperature, the minimum extent is always inversely proportional to the density.
- For two chosen densities in both directions, there is a minimum radial extent for the onset of improvement and it is less than the optimal extent.
- Friction torque and maximum temperature can only be improved marginally.
- Around ½ of the pad should be textured to minimize the friction torque for a small convergence ratio.
- The maximum temperature is minimized when the maximum pressure and temperature points are closer, and the extent in the radial direction will be higher than 87,5%.

REFERENCES

[1] H. Yang, S. Ratchev, M. Turitto, and J. Segal, “Rapid manufacturing of non-assembly complex micro-devices by microstereolithography,” *Tsinghua Science & Technology*, vol. 14, no. S1, pp. 164–167, Jun. 2009, doi: 10.1016/s1007-0214(09)70086-0.

[2] V. G. Marian, G. Dumitru, G. Knoll, and S. Filippone, “Theoretical and experimental analysis of a laser textured thrust bearing,” *Tribology Letters*, vol. 44, no. 3, pp. 335–343, Sep. 2011, doi: 10.1007/s11249-011-9857-8.

[3] M. B. Dobrica and M. Fillon, “About the validity of Reynolds equation and inertia effects in textured sliders of infinite width,” *Proceedings of the Institution of Mechanical Engineers, Part J: Journal of Engineering Tribology*, vol. 223, no. 1, pp. 69–78, Jan. 2009, doi: 10.1243/13506501jet433.

[4] C. I. Papadopoulos, P. G. Nikolakopoulos, and L. Kaiktsis, “Evolutionary optimization of Micro-Thrust bearings with periodic partial trapezoidal surface texturing,” *Journal of Engineering for Gas Turbines and Power*, vol. 133, no. 1, Sep. 2010, doi: 10.1115/1.4001990.

[5] C. I. Papadopoulos, E. E. Efstathiou, P. G. Nikolakopoulos, and L. Kaiktsis, “Geometry optimization of textured Three-Dimensional micro- thrust bearings,” *Journal of Tribology*, vol. 133, no. 4, Oct. 2011, doi: 10.1115/1.4004990.

[6] D. Fouflias, A. Charitopoulos, C. I. Papadopoulos, L. Kaiktsis, and M. Fillon, “Performance comparison between textured, pocket, and tapered-land sector-pad thrust bearings using computational fluid dynamics thermohydrodynamic analysis,” *Proceedings of the Institution of Mechanical Engineers, Part J: Journal of Engineering Tribology*, vol. 229, no. 4, pp. 376–397, Sep. 2014, doi: 10.1177/1350650114550346.

[7] C. I. Papadopoulos, L. Kaiktsis, and M. Fillon, “Computational fluid dynamics Thermohydrodynamic analysis of Three-Dimensional Sector-Pad thrust bearings with rectangular dimples,” *Journal of Tribology*, vol. 136, no. 1, Oct. 2013, doi: 10.1115/1.4025245.

[8] A. Dadouche, M. Fillon, and J.-C. Bligoud, “Experiments on thermal effects in a hydrodynamic thrust bearing,” *Tribology International*, vol. 33, no. 3–4, pp. 167–174, Apr. 2000, doi: 10.1016/s0301-679x(00)00023-2.

[9] A. Dadouche, M. Fillon, and W. Dmochowski, “Performance of a Hydrodynamic Fixed Geometry Thrust Bearing: Comparison between Experimental Data and Numerical Results,” *Tribology Transactions*, vol. 49, no. 3, pp. 419–426, Sep. 2006, doi: 10.1080/10402000600781457.

[10] D. Gropper, T. J. Harvey, and L. Wang, “A numerical model for design and optimization of surface textures for tilting pad thrust bearings,” *Tribology International*, vol. 119, pp. 190–207, Mar. 2018, doi: 10.1016/j.triboint.2017.10.024.

[11] D. Gropper, T. J. Harvey, and L. Wang, “Numerical analysis and optimization of surface textures for a tilting pad thrust bearing,” *Tribology International*, vol. 124, pp. 134–144, Aug. 2018, doi: 10.1016/j.triboint.2018.03.034.

[12] G. Stachowiak and A. W. Batchelor, *Engineering Tribology*. Butterworth-Heinemann, 2005.

[13] A. Dadouche, M. Fillon, and W. Dmochowski, “Performance of a Hydrodynamic Fixed Geometry Thrust Bearing: Comparison between Experimental Data and Numerical Results,” *Tribology Transactions*, vol. 49, no. 3, pp. 419–426, Sep. 2006, doi: 10.1080/10402000600781457.

[14] K. Mostefa, D. Souchet, D. Zebbar, and A. Youcefi, “Effects of the dimple geometry on the isothermal performance of a hydrodynamic textured tilting-pad thrust bearing,” *International Journal of Heat and Technology*, vol. 36, no. 2, pp. 463–472, Jun. 2018, doi: 10.18280/ijht.360211.